Synthesis, characterization and biological activity of new thioamide Schiff base complexes

Mohamed Adel Rady, Dr.Jehan A hassanen, Dr.Nader Y. F. Hassan

Abstract— New metal complexes of Ni(II), Zn(II) and Cu(II) with the Schiff base(2-((E)-2-hydroxy-5-((E)-m-tolyldiazenyl)-3-((E)-p-tolyldiazenyl)benzylidene)hydrazine-1-carbothioamide),(H_2L) have been prepared and characterized by elemental and thermal analyses, FT-IR, UV–Vis, XRD analysis, SEM analysis, ^{1}H-NMR, and C^{13} as well as conductivity and magnetic moments measurements. The IR spectra showed that the ligand acts as neutral bi-dentate ligand. The geometries of metal complexes were either octahedral or square pyramidal. The effect of the presence of an azo group on the biological activity of the ligand was investigated. The ligand and its complexes are biologically inactive due to the presence of azo-group.

Index Terms— Spectroscopic study, SEM, XRD, Cytotoxicity.

DOI: 10.31838/ecb/2023.12.5.352

1 INTRODUCTION

Many Schiff base transition metal complexes are reported to have anticancer and antimicrobial activities[1–3]. It was reported that some drugs have greater activity when administered as metal complexes than that as free organic compounds[4]. Hence, Schiff base transition metal complexes may be an untapped reservoir for drugs[5,6]. Recently, complexes of transition and non-transition metals with Schiff base ligands are promising materials for electronic applications due to their outstanding photo and electroluminescent (PL and EL) properties, and the ease of synthesis that readily allows structural modification for optimization of material properties[7–10] .

Hydrazine and substituted hydrazine complexes of oxocations have not been previously investigated. The coordination chemistry of hydrazine and substituted hydrazine is of special interest because of the variety of ways in which these species can be bonded to metal ion: e.g., as uni-dentate, bi-dentate or bridging and sometimes act as tridentate[11]. An enormous number of sulfone subsidiaries have been discovered wide assortment of pharmacological activities[12]. As well a that the bis heterocyclic compounds of quinazoline and imidazolidine derivatives are known as antifungal and antitumor agents[13,14].

2. EXPERIMENTAL

2.1 Materials and Method

Melting points were determined by the capillary tube on an electro thermal apparatus. The ^{1}H and ^{13}C NMR spectra were recorded on a Bruker Avance II400 MHz spectrophotometer and characterized by chemical shifts (ppm) relative to internal standard tetramethyl silane (TMS) and J values (hertz). Elemental analyses were carried out on a Perkin-Elmer Analyzer, and the measured data were within ±0.31% of the calculated values for C, H and N. IR spectra were recorded on Bruker FTIR Spectrophotometer (4000–400 cm-1) in KBr pellets and/or by Genesis II FTIR Spectrometer in the (4000–400 cm-1) range with 40 scans in KBr discs. The X-ray diffraction (XRD) analysis was conducted by using a Bruker D8 X-ray diffractometer with Cu-Kα radiation (λ = 1.5418 Å) in the range of 10–70° and the scanning rate of 1.5°/min. A scanning electron microscope (SEM) was applied to observe the surface morphology of nanoparticles using a Hitachi S4160 instrument. Thermogravimetric analyses (TG) carried out in the temperature range from 25 to 800 oC in a steam of nitrogen atmosphere by Shimadzu TGA 50 H thermal analysis. The experimental conditions were: platinum crucible, nitrogen atmosphere with a 30 ml/min flow rate and a heating rate 10 oC/min. Rigaku 8150 thermoanalyser under dynamic nitrogen atmosphere, at a heating rate of 5 deg min–1 was also used beside the above apparatus. Solvents that used for the chemical reactions are obtained from commercial sources, were of analytical grade and used without further purification..

2.2 Synthesis of ligand

Hydrazine ligand (2-((E)-2-hydroxy-5-((E)-m-tolyldiazenyl)-3-((E)-p-tolyldiazenyl) benzylidene) hydrazine-1-carbothioamide), (H_2L) was prepared from reaction of 2-hydroxy-3,5-bis((E)-p-tolyldiazenyl)benzaldehyde and thiosemicarbazide.

A certain amount of 2-hydroxy-3,5-bis((E)-p-tolyldiazenyl)benzaldehyde (1) (1.45 g, 5.12 mmol) and thiosemicarbazide (0.62 mL, 5.11 mmol) were dissolved in a hot dry ethanol (20 mL) containing catalytic amount of anhydrous sodium acetate (0.75 g, 9.14 mmol). Thereafter, the reaction mixture was heated under stirring and reflux for 5 h. The reaction progress was followed by TLC to investigate the disappearance of (1) and consequently reaction completion. After the disappearance of (1), the reaction mixture then cooled to room temperature and then poured into an ice-water mixture. The product then collected, dried and crystallized from hot ethanol to afford brown crystals of the desired ligand

- *Mohamed Adel Rady , Department of Chemistry , faculty of science , Port-said university , E-mail : mohamed.rady@sci.psu.edu.eg.*
- *Dr.Jehan A. Hassanen , Professor of organic chemistry, Department of Chemistry , faculty of science ,Suez-canal university.*
- *Dr. Nader Y. F. Hassan , Assistant Professor of analytical chemistry , Department of Chemistry , faculty of science , Port-said university, E-mail : nader.hassan@psu.edu.eg.*

(2-((E)-2-hydroxy-5-((E)-m-tolyldiazenyl)-3-((E)-p-tolyldiazenyl)benzylidene)hydrazine-1-carbothioamide),[(H_2L) (2)]. Yield 71%; mp 235–242 °C. FTIR (KBr, cm-1): 3412 (s, sh), 3260 (m, br), 3173 (s, br), 2820 (s, sh), , 1794 (vs, sh), 1524 (s, sh), 1569 (s, sh), 1490 (w, sh), 1482 (s, sh), 1370 (m, sh), 1303 (s, sh), 1248 (s, sh), 1213 (w, sh), 1071 (w, sh), 1036 (s, sh), 969 (m, sh), 833 (m, sh), 787 (m, sh), 731 (m, sh), 694 (m, sh), 629 (m, sh), 531 (s, sh). 1H NMR (400 MHz, DMSO-d6) δ (ppm): 7.46,7.49 (m, 3H, Ar-H), 7.77,7.79 (m, 2H, Ar-H), 8.42 (s,1H, CH=N), 12.01 (s, 1H, NH)ppm .13C NMR (100 MHz, DMSO-d6) δ (ppm): 174.66 (C=S), 165.83 (C=O), 156.73 (C=N), 134.65,131.55,129.63, 128.11(C-aromatics), EI-MS: m/z 292.20 ([M]+·, 68%). Anal. Calcd for C22H25N7OS (M=435.92 g/mol): C,60.56; H, 5.73; N,22.48; S,7.34 %. found C, 60.43; H, 5.54; N, 22.33; S, 7.12%.

2.2.1 Preparation of H_2L complexes (3a-c):

The following steps were used to prepare H_2L complexes (3a-c). A hot aqueous ethanolic solution (1:1, 25 mL) of the divalent metal salt ($MCl_2.xH_2O$; $NiCl_2.6H_2O$, $CuCl_2.4H_2O$, $ZnCl_2$) (1 mmol) was added to a hot ethanolic solution (25 mL) of H_2L (0.265 g, 1 mmol) containing few drops of ammonium hydroxide (pH 9.2). The reaction mixture heated under reflux for 2 h. Thereafter, the solvent was partially evaporated under a reduced pressure and then the reaction mixture was cooled to room temperature to allow the precipitation of the desired products. These products were filtered, washed with H_2O (5 mL x 3), warm EtOH (5 mL x 2) and Et_2OH (5 mL x 3) successively, and dried in *vacuo*.

[Ni(H_2L)].2H_2O (3a): yellow-brown powder (63%). FTIR (KBr, cm^{-1}): 3421 (s, sh), 2601 (w, br), 1616 (vs, sh), 1579 (s, sh), 1536 (s, sh), 1489 (s, sh), 1393 (m, sh), 1338 (s, sh), 1276 (m, sh), 1243 (s, sh), 1184 (w, sh), 1147 (m, sh), 1072 (m, sh), 1022 (w, sh), 986 (w, sh), 853 (w, sh), 799 (m, sh), 773 (m, sh), 615 (s, sh), 496 (s, sh), 400 (m, sh). EI-MS: m/z 431.20 ([M]$^{+\cdot}$, 35%). Anal. Calcd. for $C_{22}H_{27}N_7O_3SNi$ (M = 465.23 g/mol): C, 57.74; H, 6.8; N, 22.06; S, 7.88%. Found: C, 57.63; H, 6.6; N, 21.96; S, 7.74%.

[Cu(H_2L)].4H_2O (3b): Reddish-brown powder (68%). FTIR (KBr, cm^{-1}): 3449 (s, sh), 3346 (s, sh), 1584 (s, sh), 1537 (s, sh), 1437 (m, sh), 1393 (m, sh), 1246 (s, sh), 1205 (m, sh), 1150 (m, sh), 1074 (w, sh), 991 (m, sh), 896 (m, sh), 848 (w, sh), 758 (m, sh), 600 (w, sh), 514 (w, sh), 479 (m, sh), 451 (w, sh). EI-MS: m/z 435.20 ([M]$^{+\cdot}$, 35%). Anal. Calcd. for $C_{22}H_{27}N_7O_3SCu$ (M = 498.34 g/mol): C, 57.31; H, 6.2; N, 21.85; S, 7.54%. Found: C, 57.22; H, 6.04; N, 21.63; S, 7.47%.

[Zn(H_2L)Cl].2H_2O (3c): Yellowish-white powder (58%). FTIR (KBr, cm^{-1}): 3506 (s, br), 3350 (m, sh), 3301 (m, sh), 3102 (m, br), 2927 (m, sh), 2589 (w, br), 1618 (s, sh), 1574 (s, sh), 1456 (s, sh), 1367 (m, sh), 1343 (m, sh), 1256 (s, sh), 1206 (m, sh), 1169 (m, sh), 1144 (m, sh), 1085 (m, sh), 988 (m, sh), 905 (m, sh), 853 (m, sh), 801 (m, sh), 724 (m, sh), 600 (w, sh), 575 (w, sh), 548 (m, sh), 519 (m, sh), 461 (m, sh). EI-MS: m/z 399.20 ([M]+·, 35%). Anal. Calcd. for $C_{22}H_{27}N_7O_3SZn$ (M = 499.14 g/mol): C, 57.26; H, 6.13; N, 21.73; S, 7.34%. Found: C, 57.25; H, 6.06; N, 21.67; S, 7.25%.

The conductivity of complexes was measured and found in the range between (2.630×10^{-8}- 9.772×10^{-11})$\Omega^{-1}cm^{-1}$

3. Results and Discussion

Schiff base ligand (H_2L, **3**) was prepared from the –hydroxy 3,5-bis((E)-p-tolyldiazenyl)benzaldehyde as a starting material through consecutive steps outlined in (Scheme 1).

Nickel(II), copper(II), and zinc(II) complexes of the H_2L ligand (M(II)H_2L, 3a-c) were synthesized by refluxing mixtures of the deprotonated H_2L and metal chlorides in aqueous ethanol (**Scheme 1**). The deprotonation of the H_2L was performed using ammonium buffer solution (pH 9.2).

The parent ligand and its complexes were obtained in acceptable yields. The structures of these new compounds were investigated based upon elemental and spectral analysis (FTIR, NMR (^1H, ^{13}C), EI-MS) as well as thermal and XRD analysis.

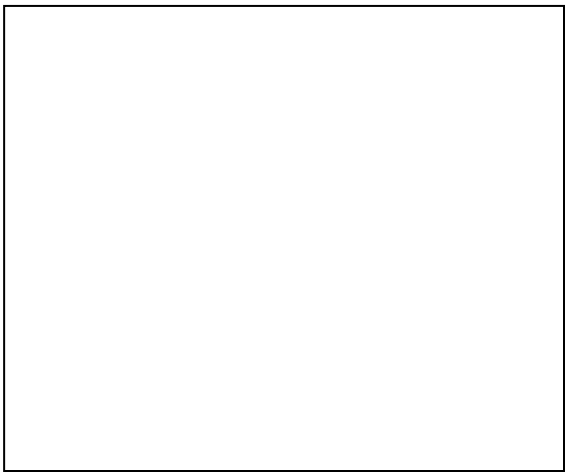

3.1 Structural Characterization

3.1.1 Microanalytical data and mass spectrometry

The parent ligand (H_2L) and its chelates (M(II)H_2L) have displayed satisfying elemental analyses which is consistent with the proposed molecular formulas for them (see experimental part). Meanwhile, the electron impact mass spectra (EI-MS) of H_2L and M(II)H_2L complexes showed dominant peaks for the molecular ions as a result of the departure of a single electron from the parent molecules.

3.1.2 FTIR

The FTIR spectra of the free Schiff base ligand (H_2L, HL) and its metal M(II)-complexes are shown in Fig. 1. In the spectrum of H_2L, the IR peaks distinctive for the phenolic O-H and azomethine groups of the Schiff base segment were observed at 3581 and 1611 cm−1, respectively. On the other hand, the ν(C=O), thioamide IV ν(C=S), νas(NCS), and νs(NCS) of the

thiohydantoin moiety were observed at 1712, 1194, 1488, 745 cm−1, respectively . Moreover, The two strong stretches at 1532 and 1330 cm−1 are assigned to the thioamide I and II modes, respectively . The emergence of a weak IR band at 2598 cm−1 in the spectrum of H_2L, attributable to the ν(S–H) stretching vibration, confirms the minor contribution of thiol form in the thiol↔thione tautomeric equilibrium in the solid structure of H_2L. These FTIR spectral results prove the successful formation of thioamide Schiff base (H_2L, **3A**) ligand. Noteworthy, in the spectra of H_2L complexes, the phenolic O-H band has disappeared and the ν(Aryl–O) band was red-shifted by 15-18 cm−1. These finding suggest the deprotonation of phenolic OH group and participation of the aryl-O in chelation of metal ions in comparison to the values for the native H_2L. These downward shifts in wavenumber values are indicative for the coordination of the carbonyl-O of thiohydantoin segment and an imine-N to metal ions. It could be realized that the H_2L have coordinated to Ni(II) and Cu(II) ions via the phenolic-O, carbonyl-O, and and amine-N in the spectra of Ni(II)-/ Cu(II)-H_2L complexes. Whereas, in Zn(II) complex, emergence of the thiol peak (2601 cm−1) is an indicative for the contribution of thiol form in coordination. Noticable, the positions of ν(C=S), νas(NCS), and νs(NCS) peaks kept almost unchanged in the spectra of complexes, ruling out the sharing of sulphur atom in coordination to metal ions. Overall, based on IR spectral findings, H_2L acts as a monoanionic (ONS) tridentate ligand.

This suggestion is further confirmed by the emergence of new IR bands in the ranges of 519–514 and 479–496 cm−1 assigned for ν(M–O) of two different types of M–O bonds as well as new peaks in the range of 451–461 cm−1 characteristic for ν(M–N). The hydrated nature of M(II)-H_2L, as suggested by the analytical data, was reflected from the growth of new absorption bands at 3463 ± 42 cm−1 ascribed to ν(O-H) band. Moreover, the two characteristic peaks around 750 and 640 cm−1 are attributed to ϱr(H_2O) and ϱw(H_2O), respectively, for the coordinated water molecules.

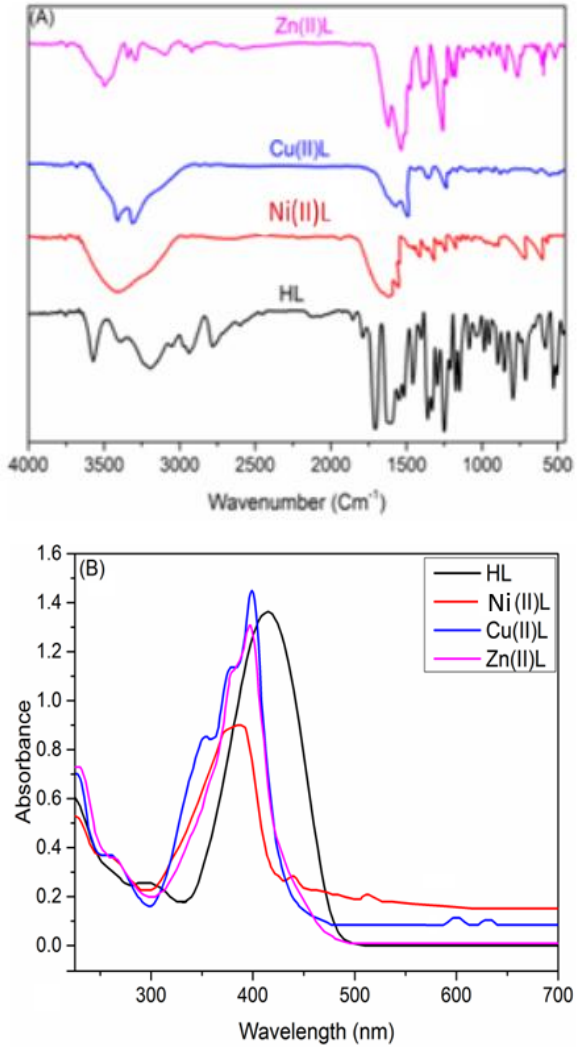

Fig. 1 : (A) FTIR spectra of the parent ligand (H_2L) and its chelates (M(II)H_2L, M(II)L) for illustrating of the changes in the positions and/ or intensities of the carbonyl, imine, and phenolate stretches in the spectrum of H_2L owing to coordination with metal(II) ions.

(B) UV-Vis spectra of the free HL ligand and its complexes in DMSO (10–3 M).

3.1.3 UV-Vis spectra

Fig. 1B shows the electronic absorption spectra for the solutions of H_2L and its M(II) complexes in DMSO (10–4 M). It can be noticed that the spectrum of H_2L was dominated by two main absorption peaks. The first peak was observed at 267 nm that assigned to π→π* transition of the heterocyclic and/or phenyl moieties. The second one appeared around 369 nm which can be ascribed to the n→π* transition involving all electron-possessing groups in the ligand (such as C=O, C=S, and C=N). In the electronic spectra of M(II)H_2L complexes, the main absorption peaks have hypsochromically shifted relative to the corresponding ones in the native H_2L, supporting the

coordination of anionic form of H_2L ligand with metal(II) ions . The electronic spectrum of Ni(II)H_2L complex displays π→π*, n→π*, and d→d transitions bands. It can be seen the d-d bands centered at 511 and 432 nm which have been assigned to 6A1g→4T2g(G) and 6A1g→4T1g(P) transitions, respectively. These findings coupled with the value of magnetic moment for Ni(II) complex (5.81 B.M) demonstrate the high spin d5 configuration for Ni(II) ion and consequently paramagnetism of its complex as well as an octahedral geometry around Ni(II) ion . Also, the electronic spectrum of Cu(II)H_2L complex shows the native π→π* and n→π* bands of the parent ligand but with hypsochromic shifts, as well as relatively weak and broad peaks centered at 579 and 648 nm which are distinctive for the d→d electronic transitions of type 2B1g + 2A1g and 2B1g→2Eg transitions. Based on these results, the square planar geometry has proposed for Cu(II) ion in the Cu(II)H_2L complex. Furthermore, the magnetic moment of Cu(II) complex was found to be 1.81 B.M which in matching with that assigned for the square planar Cu(II) complexes . As the Zn(II) has a fully filled d-orbit (d10), it is expected that the Zn(II)H_2L complex is diamagnetic and do not have any d-d transitions,. In this respect, the spectrum of the Zn(II)H_2L complex displayes only high-energy absorption bands at 263 and 294 nm due to π→π* and n→π* transitions (shifted by –20 nm comparative to the parent ligand). Based on the electronic spectral data, it could be concluded that the Zn(II) complex had a tetrahedral geometry.

3.1.4 NMR spectroscopy

The ^1H and ^{13}C NMR assignments confirm the successful preparation of the parent ligand, thioamide Schiff base (H_2L). The ^1H NMR spectrum of H_2L (Fig.) shows three singlets at δ 12.81, 12.05, 10.03 ppm attributable for the resonance of thioamide and phenolic protons, respectively. The protons of phenyl group are displayed as two doublets and a singlet at the range of δ 7.48–6.28 ppm. The methylene (of thiohydantoin moiety) and methyl groups are represented two singlets at δ 4.00 and 2.95 ppm, respectively. Further evidence for the structure of spectrum of H_2L was obtained from its ^{13}C NMR spectrum (Fig.). Where the three very low-field signals at δ 173.96, 166.27, 164.69 ppm are assigned to the thiocarbonyl, azomethine, and carbonyl groups, respectively. The phenolic carbon signals can be seen at δ 161.50 and 161.26 ppm. A set of proton peaks observed at the range of δ 131.02–103.29 ppm are assigned to the resonance of phenyl carbons. The resonances of methylene and methyl carbons were presented at δ 33.87 and 14.61 ppm, respectively.

3.1.5 Thermal analysis

3.1.5.1 Thermogravimetric analysis of the ligand (H_2L) and its complexes

The thermal stabilities of the M(II)-H_2L chelates were investigated by using thermogravimetric analysis (TGA) as shown in Fig. 48A, differential thermogravimetry (DTG) (Fig. 48B), and differential thermal analysis (DTA) (Fig. 48C) techniques at the temperature range from the ambient temperature up to 800 °C under an inert nitrogen atmosphere. The phases of thermal degradation, corresponding temperature ranges, DTG peak temperature, and the fragments lost in each decomposition stage as well as their respective weight loss (WL)percentages are given in Table 1.

TABLE 1

THERMAL BEHAVIOR OF CARBOTHIOAMIDE SCHIFF BASE LIGAND (H_2L, 6A) AND ITS TRANSITION METAL COMPLEXES (M(II)H_2L, 6A-C)

Sample MF (MW)	DTG peak (°C)	Temp rang (°C)	Fragment lost (FW)	W% Found (Calcd.)
$C_{22}H_{25}N_7OS$	50-250	200	$3NH_3$ +NO	23.55 (23.45)
	250-700	500	$7C_2H_2$+CS+N_2	41.41 (41.60)
Ni(II)H_2L	50-200	150	$2H_2O$+NH_3	20.96 (20.45)
$C_{22}H_{27}N_7O_3SNi$	200-500	300	$8C_2H_2$+CS+NO	48.63 (47.60)
Cu(II)H_2L	50-260	190	$2H_2O$+$2NH_3$	23.43 (23.21)
$C_{22}H_{27}N_7O_3SCu$	260-600	390	$8C_2H_2$+CS+$2N_2$	50.32 (50.12)
Zn(II)H_2L	40-280	240	$2H_2O$+NH_3+N_2	31.54 (31.25)
$C_{22}H_{27}N_7O_3SZn$	280-700	420	$10C_2H_2$+CS+$2N_2$	58.63 (57.94)

revealed its thermal stability up to 50 °C and begins to loss of $3NH_3$ +NO (WL 23.55%) within the temperature range 50-250°C with a relatively broad DTG peak centered at 120 °C. With increasing the temperature, the ligand was further decomposed to loss of $7C_2H_2$+CS+N_2 (WL 41.41%) in the temperature range 250-700°C .The thermogram of Ni(II)-H_2L displays four successive thermal degradation stages. The first stage was in the range of 50-200 °C with a broad DTG peak centered at 110°C (WL 20.96%), attributable to the departure of $2H_2O$+NH_3 from the Ni(II) complex. Further heating of Ni(II) complex resulted in the loss of $8C_2H_2$+CS+NO in temperature range 200-500 °C, as a second decomposition phase.The hydrated nature of Cu(II)-H_2L complex can be confirmed from its TG curves which show the volatilization of $2H_2O$+$2NH_3$ in the foremost thermal decomposition stage ranged from 50-260 °C (**Fig. 2A**) with a broad DTG peak (**Fig. 2B**). Moreover, the thermogram of Cu(II) complex shows other two decomposition phases at higher temperatures (260-600°C) and assigned to the loss of $8C_2H_2$+CS+$2N_2$.

The TG patterns of Zn(II)-H_2L complex indicate that it is thermally decomposed over two stages; The first process spreads over a wide range of temperature intervals (40-280°C). On the other hand, the second step is a wide range of temperatures (280-700°C).

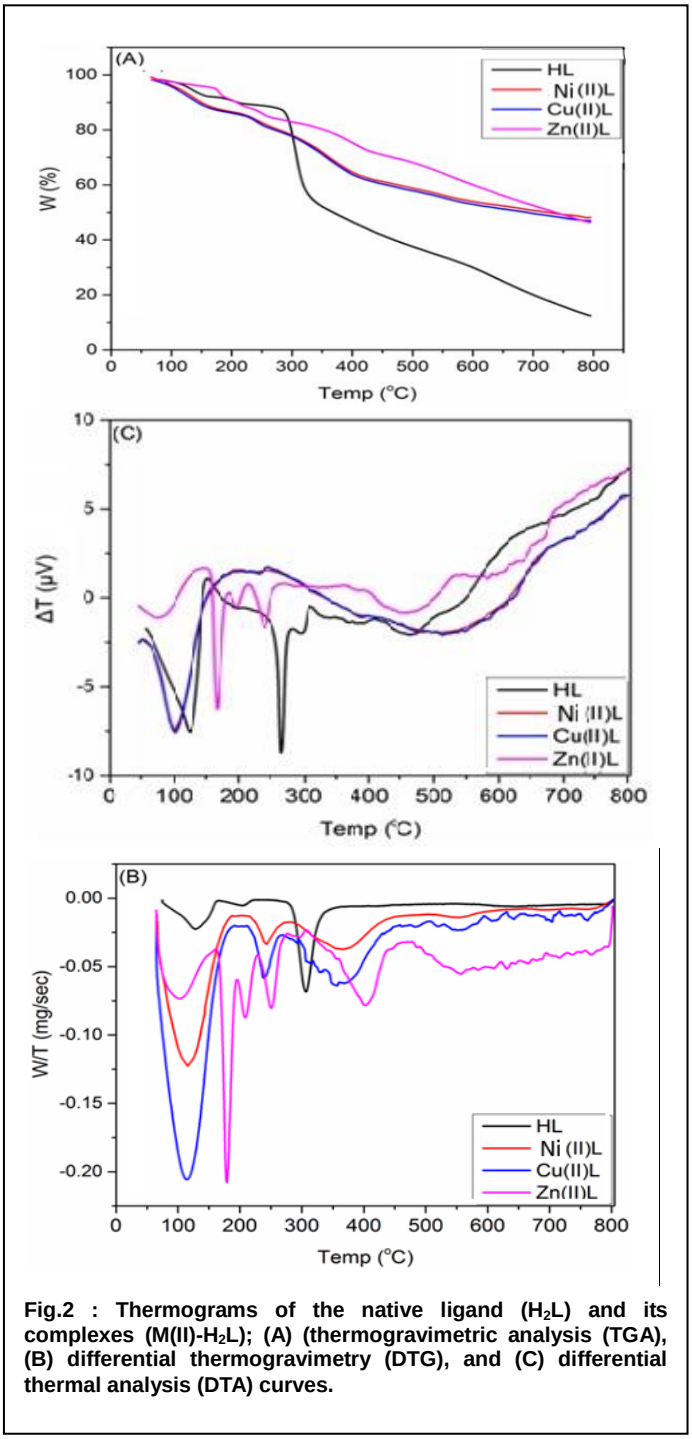

Fig.2 : Thermograms of the native ligand (H_2L) and its complexes (M(II)-H_2L); (A) (thermogravimetric analysis (TGA), (B) differential thermogravimetry (DTG), and (C) differential thermal analysis (DTA) curves.

The DTA curves of the native ligand and its complexes (Fig. 2C) display weak and broad endothermic peaks at the temperature zone just prior to or accompanying the mass loss step in the corresponding TG thermograms.

3.1.5.2 Thermodynamics data of the thermal decomposition of ligand (H_2L)

The data are summarized in (Table 2) and shown in Fig. 3. The activation energies of decomposition ligand (H_2L) found to be in the range 3.12.104 - 5.75.104 kJmol-1. The high values of the activation energies reflect the thermal stability of the ligand . The entropy of activation found to have negative values, which indicate that the decomposition reactions proceed with a lower rate than the normal ones. The correlation coefficients of the Arrhenius plots of the thermal decomposition steps found to lie in the range 0.945 to 0.99 , showing a good fit with linear function.

TABLE 2

THERMODYNAMIC DATA OF THE THERMAL DECOMPOSITION OF LIGAND (H_2L)

Complex	Stage	Method	E (KJmol^{-1})	A (s^{-1})	ΔS (Jmol^{-1}K^{-1})	ΔH (KJmol^{-1})	ΔG (KJmol^{-1})	R
H_2L	1st	CR	53.10^4	1.9.10^3	-186.10^2	491.10^2	1.35.10^5	0.95
		Hm	5.75.10^4	1.64.10^4	-168.10^2	537.10^2	1.51.10^5	0.94
		Average	5.25.10^4	5.5.10^3	-177.10^2	5.135..10^2	1.43.10^5	0.945
	2nd	CR	3.12.10^4	3.42.10^2	-260.10^2	25.10^4	1.88.10^5	0.99
		Hm	3.72.10^4	2.5.10^2	-243.10^2	32.10^4	1.84.10^5	0.98
		Average	3.42.10^4	1.83.10^2	-2.5.10^2	29.10^4	1.86.10^5	0.985

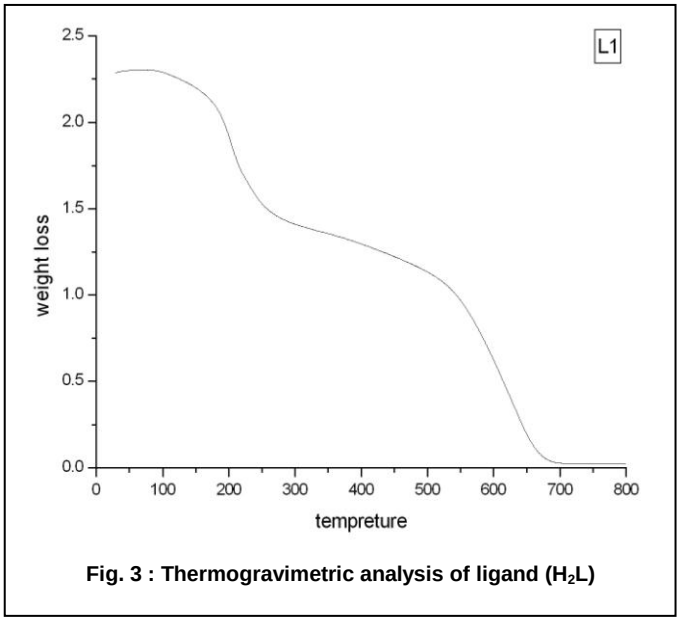

Fig. 3 : Thermogravimetric analysis of ligand (H_2L)

3.1.5.3 Thermodynamics data of the thermal decomposition of transition metal complexes (M(II)H_2L 6a-c)

The data are summarized in Table 3 - 5 and shown in Fig. 4-5. The activation energies of decomposition found to be in the range 2.83.104 - 5.85.104 kJmol-1, 2.24.104 - 7.765.104 kJmol-1, and 5.04.104 - 9.15.104 kJmol-1 for Ni(II)H_2L , Cu(II)H_2L, and Zn(II)H_2L respectively. The high values of the activation energies reflect the thermal stability of the complexes. The entropy of activation found to have negative values in all the complexes, which indicate that the decomposition reactions proceed with a lower rate than the normal ones. On another meaning the thermal decomposition processes of all complexes are non-spontaneous, i.e., the complexes are thermally stable. The correlation coefficients of the Arrhenius plots of the thermal decomposition steps found to lie in the

range 0.895 to 0.993 , showing a good fit with linear function.

TABLE 3

THERMODYNAMIC DATA OF THE THERMAL DECOMPOSITION OF NI COMPLEX NI(II)H_2L.

Complex	Stage	Method	E (KJmol^{-1})	A (s^{-1})	ΔS (Jmol^{-1}K^{-1})	ΔH (KJmol^{-1})	ΔG (KJmol^{-1})	R
Ni(II)H_2L	1st	CR	$2.83.10^4$	$4.99.10^1$	$-2.14.10^2$	$2.54.10^4$	$1.01.10^4$	**0.933**
		Hm	$3.27.10^4$	$4.15.10^2$	$-1.96.10^2$	$2.98.10^4$	$9.82.10^4$	**0.934**
		Average	$3.55.10^4$	$2.32.10^2$	$-2.05.10^2$	$2.76.10^4$	$5.42.10^4$	**0.9335**
	2nd	CR	$5.18.10^4$	$3.28.10^3$	$-1.81.10^2$	$4.81.10^4$	$1.29.10^5$	**0.98**
		Hm	$5.85.10^4$	$4.26.10^4$	$-1.602.10^2$	$5.48.10^4$	$1.26.10^5$	**0.99**
		Average	$5.515.10^4$	$2.294.10^4$	$-1.706.10^2$	$5.145.10^4$	$1.275.10^5$	**0.985**

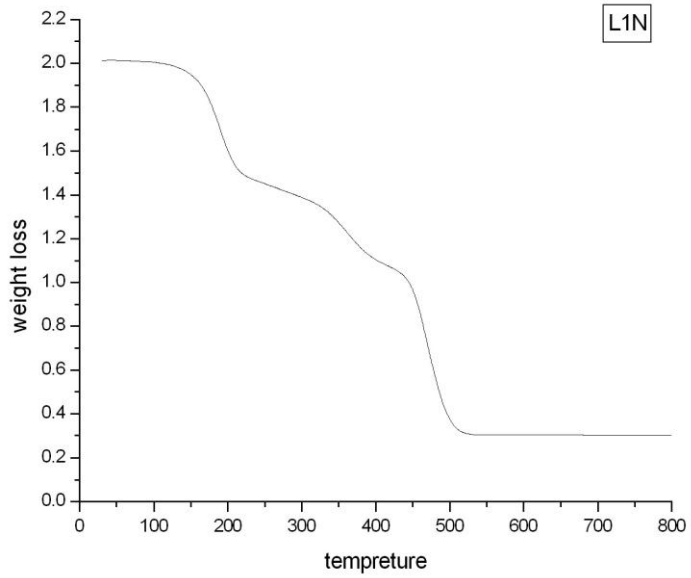

Fig. 4 : Thermogravimetric analysis of Ni(II)H_2L

TABLE 4

THERMODYNAMIC DATA OF THE THERMAL DECOMPOSITION OF CU COMPLEX CU(II)H_2L.

Complex	Stage	Method	E (KJmol^{-1})	A (s^{-1})	ΔS (Jmol^{-1}K^{-1})	ΔH (KJmol^{-1})	ΔG (KJmol^{-1})	R
Cu(II)H_2L	1st	CR	$2.24.10^4$	$2.3.10^0$	$-2.41.10^2$	$1.91.10^4$	$1.15.10^5$	**0.932**
		Hm	$3.04.10^4$	$3.68.10^1$	$-2.17.10^2$	$2.7.10^4$	$1.14.10^5$	**0.952**
		Average	$2.64.10^4$	$1.9415.10^1$	$-2.29.10^2$	$2.305.10^4$	$1.145.10^5$	**0.947**
	2nd	CR	$4.61.10^4$	$1.36.10^5$	$-1.51.10^2$	$7.17.10^4$	$1.51.10^5$	**0.97**
		Hm	$7.29.10^4$	$4.35.10^5$	$-1.42.10^2$	$7.48.10^4$	$1.49.10^5$	**0.968**
		Average	$7.765.10^4$	$2.958.10^5$	$-1.47.10^2$	$7.325.10^4$	$1.5.10^5$	**0.969**

TABLE 5

THERMODYNAMIC DATA OF THE THERMAL DECOMPOSITION OF ZN COMPLEX ZN(II)H_2L.

Complex	Stage	Method	E (KJmol^{-1})	A (s^{-1})	ΔS (Jmol^{-1}K^{-1})	ΔH (KJmol^{-1})	ΔG (KJmol^{-1})	R
Zn(II)H_2L	1st	CR	$8.39.10^4$	$7.19.10^6$	$-1.18.10^2$	$7.99.10^4$	$1.36.10^5$	**0.98**
		Hm	$9.15.10^4$	$7.93.10^7$	$-9.76.10^1$	$8.75.10^4$	$1.34.10^5$	**0.99**
		Average	$8.77.10^4$	$4.325.10^7$	$-1.078.10^2$	$8.37.10^4$	$1.35.10^5$	**0.985**
	2nd	CR	$4.55.10^4$	$1.44.10^1$	$-2.29.10^2$	$4.05.10^4$	$1.77.10^5$	**0.95**
		Hm	$5.54.10^4$	$2.16.10^2$	$-2.06.10^2$	$5.04.10^4$	$1.74.10^5$	**0.96**
		Average	$5.045.10^4$	$1.152.10^2$	$-2.175.10^2$	$4.545.10^4$	$1.755.10^5$	**0.955**

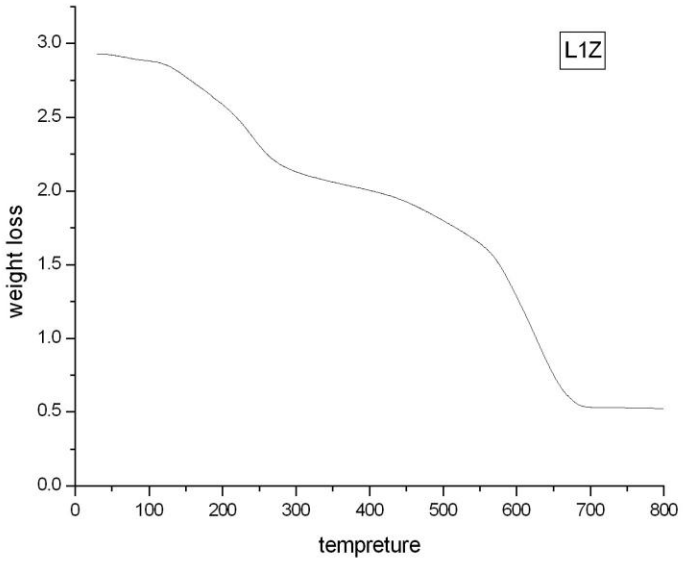

Fig. 5 : Thermogravimetric analysis of Zn(II)H_2L

3.1.6 XRD analysis

The nature of H_2L and its complexes were also obtained by powder X-ray diffraction studies. The X-ray diffractions of H_2L and its complexes are shown in Fig. 6 - 9. From the observed d XRD patterns, the grainsize of the ligand and its complexes were calculated from Schererr's formula, d XRD = 0.9k/bCosh, where d XRD is the particle size, k is the wave length of X-ray

radiation, b is the full-width half maximum and h is the diffraction angle for the hkl plane. The ligand, Ni(II), Cu(II) and Zn(II) complexes are nanocrystalline with grain size of HL, Ni(II), Cu(II) and Zn(II) complexes are nanocrystalline with grain sizes 4.7, 5.3, 3.8 and 9.7 nm respectively(Trivedi, Dahryn Trivedi and Gunin Saikia, 2015).

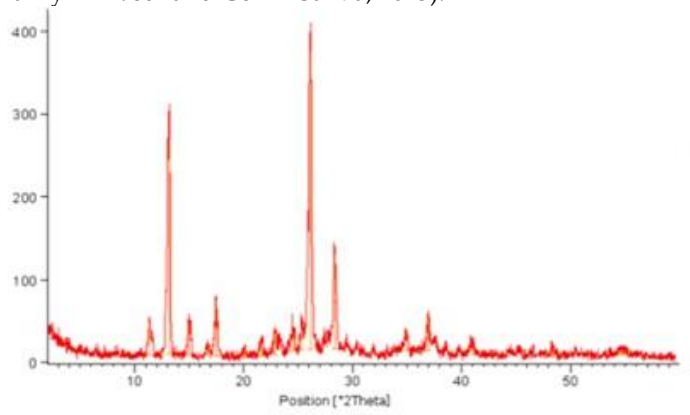

Fig. 6 : XRD analysis of ligand H_2L

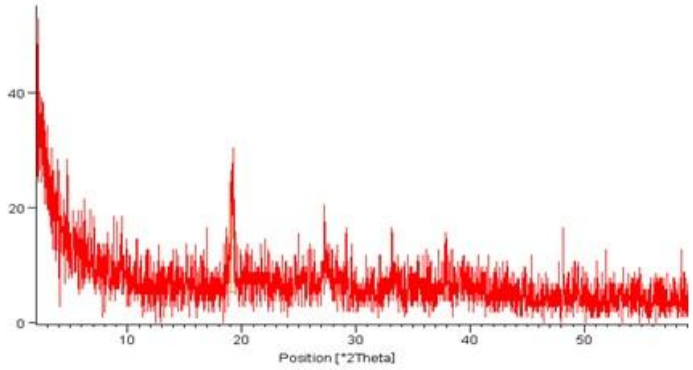

Fig. 7 : XRD analysis of Ni (II)H_2L

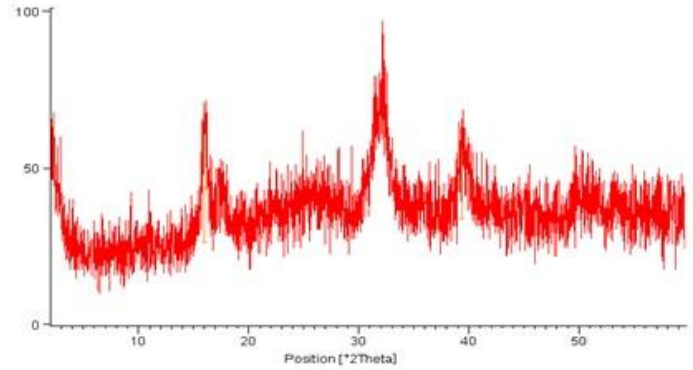

Fig. 8 : XRD analysis of Cu (II)H_2L

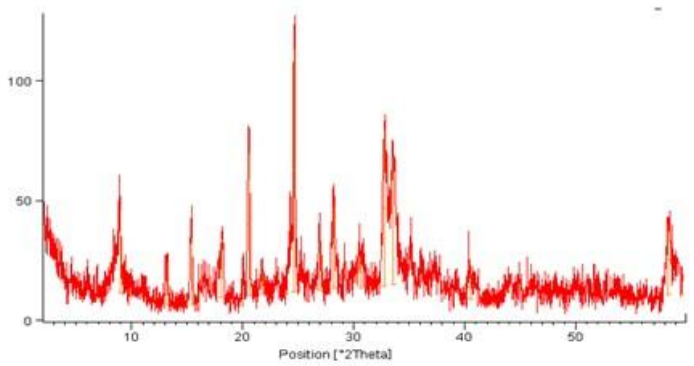

Fig. 9 : XRD analysis of Zn(II)H_2L

3.2 Morphological Characterization

The surface morphology of the free ligand and its metal complexes was investigated using SEM analysis and the obtained micrographs were collected in Fig. 10 . Noticeable, the SEM micrographs of M(II)H_2L complexes are significantly different than that for the H_2L ligand due to coordination of M(II) ions with the chelating sites for ligand (Yang et al., 2010). Furthermore, the the surface morphology of the M(II) complexes is changed with alteration of the coordinated metal ion. The micrograph of thiohydantoin Schiff base ligand (Fig. 10 A) shows non-uniform massive structures of variable sizes with some tiny particulates scattered in between. On the other hand, SEM image of Ni(II)ATSB (Fig. 10 B) displayed laminate surface with some variable-sized rods scattered on the surface. The surface of both Cu(II)ATSB and Zn(II)ATSB exhibited a high population of semispherical microparticulate which are randomly distributed over their surfaces, as shown in Fig. 10 C,D.

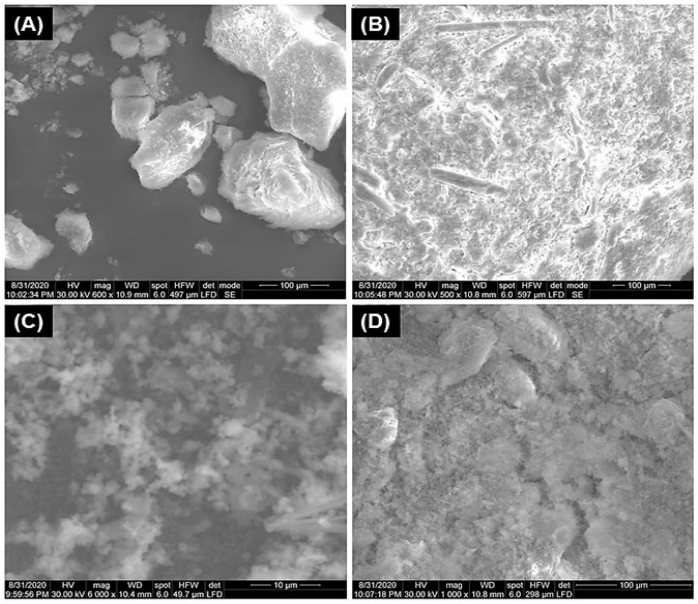

Fig. 10 : SEM micrographs of thiohydantoin Schiff base ligand (H_2L), (A); and its complexes with Ni(II), (B); Cu(II), (C); and Zn(II), (D).

3.3 In vitro anticancer study

The main aim of this work is to design safe and cytotoxic metal(II) thiohydantoin Schiff base complexes for application in the mitigation of both liver and colon cancers. To this end, the newly synthesized carbothioamide Schiff base ligand (H_2L, HL) and its metal complexes (M(II)H_2L, M(II)L) have in vitro assessed for their anticancer activity against three human cell lines (liver carcinoma *(*$HepG_2$*)*, colon carcinoma (HCT116), and normal liver cells (HL7702)*)*, in comparison with a clinical anticancer drug (Vinblastine, VBL) ($C_{46}H_{58}N_4O_9$, 810.99 g/mol).

3.3.1 In vitro cytotoxicity

The viabilities of the treated cancer cells (Fig. 11) demonstrated that all compounds have the ability to inhibit the growth of both carcinoma cells ($HepG_2$ and HCT116) with a performance depend upon; type of cancer cell, structural features of treating agent, and sample concentration.

Generally, the colon carcinoma cells (HCT116) were little more affected than the liver cells ($HepG_2$) by the new chemotherapeutic agents. For instance, the surviving HCT116 cells have decreased from 100% to 29.14% (70.86% growth reduction) after treating with 25 μg/mL of Ni(II)H_2L (Fig. 11 B). However, the $HepG_2$ cells were decreased only by 64.78% under the same remediation conditions (Fig. 11 A). Meanwhile, and further evidence for our conclusion, the IC50 values for the tested compounds were in the ranges of 22.97–2.78 μg/mL and 25.45–3.92 μg/mL against HCT116 and $HepG_2$ cells, respectively.

Noteworthy, the M(II)H_2L complexes displayed greater cancer-inhibitory effects than that induced by the native H_2L ligand. The sequence of efficacy-pattern against $HepG_2$ cells was as follow; Zn(II)H_2L (IC50 3.92±0.85 μg/mL) > Cu(II)H_2L (IC50 5.19±1.01 μg/mL) > VBL (IC50 6.83±0.75 μg/mL) > Ni(II)H_2L (IC50 7.83±0.96 μg/mL) > H_2L (IC50 25.45±1.1 μg/mL). Whilst the activity order against HCT116 cell lines was as follow; Cu(II)H_2L (IC50 2.78±0.78 μg/mL) > Zn(II)H_2L (IC50 3.41±0.89 μg/mL) > VBL (IC50 4.02±0.77 μg/mL) > Ni(II)H_2L (IC50 6.81±0.96 μg/mL) > H_2L (IC50 22.97±1.3 μg/mL).

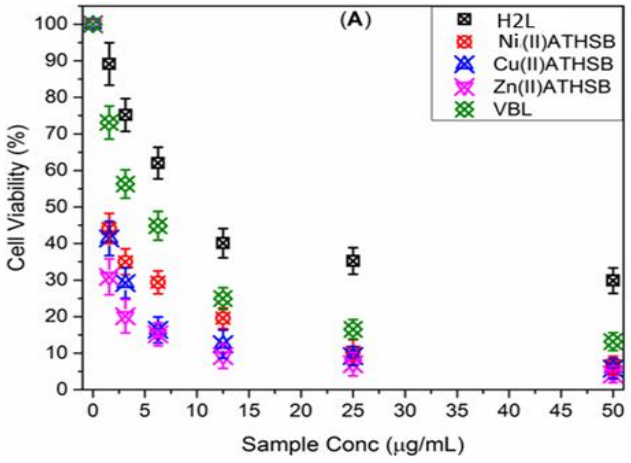

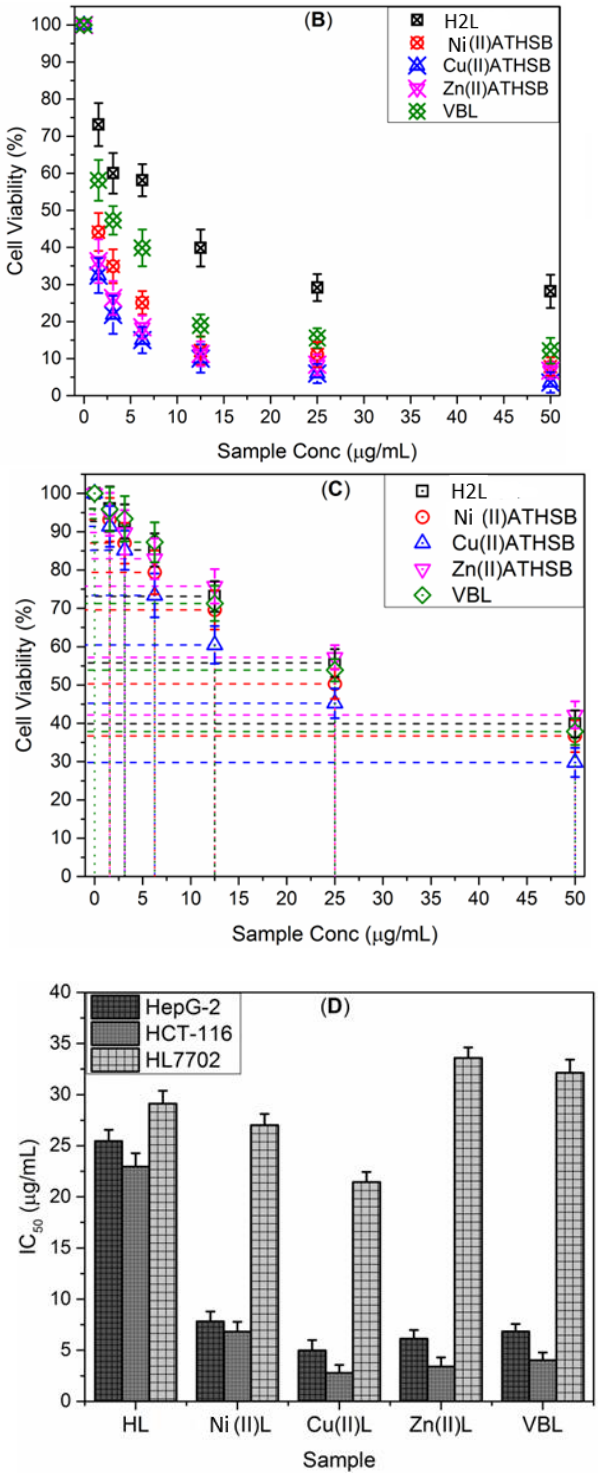

Fig. 11 : Concentration – cytotoxicity correlation for the native ligand (H_2L) and its M(II) complexes (M(II)H_2L or M(II)L; M = Ni, Cu, Zn) toward three human cell lines (A) liver carcinoma ($HepG_2$), (B) colon carcinoma (HCT116), (C) and normal liver cells (HL7702), in comparison with the clinical anticancer drug (VBL). (D) The IC50 values (μg/ mL) of the tested compounds against cancer species.

In general, the greater cytotoxic effects of M(II)H_2L complexes in comparison to the native ligand may be

attributed to an increment in the planarization of the entire molecule upon chelation of metal ions, more extended π-electron delocalization system attained with the formation of the metallocycle (Fig. 12), and an additional electrostatic interactions intrinsic due to the presence of the metal ion (Justin Dhanaraj and Johnson, 2014) .This in turns can lead to promoting the interaction between complex and cancer cell DNA through non covalent modes of action such as groove binding, π−π stacking, phosphate clamps or intercalation, resulting in dramatic changes in the DNA structure and cell death (Al-mulla, 2017). Moreover, the metal ion can selectively bind to multiple active bio-molecular targets and induces several cytotoxic mechanisms inside the cancer cell lines, dimenshing their proliferation.

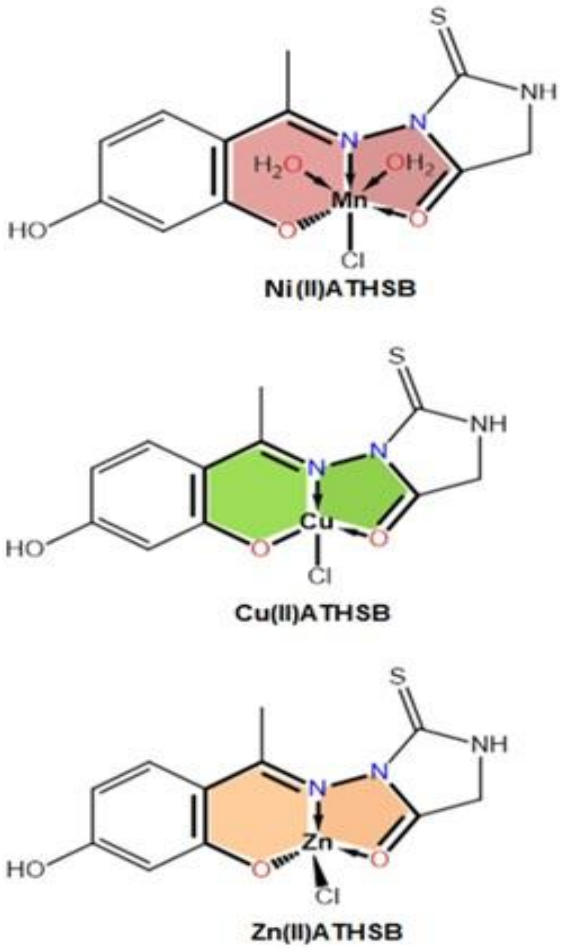

Fig. 12 : Structural and geometrical features of the new M(II)H_2L complexes showing; two types of metallocyclic rings (five-/ six-membered), all possible H-bonding acceptors (HBA) (N and O atoms of the azomethine, imidazole, and phenolic groups), H-bonding donor (HBD) sites (NH and OH imidazole, phenolic, and water fragments) and electrostatic interaction site (metal ion); those can ehnance the interaction with cancer cell DNA through π-π stacking, hydrophobic interactions, and intercalation.

The highest anti-proliferative effects of Cu(II)H_2L compared to others against colon carcinoma cells (HCT116) may be related to the great planarization of this complex (Fig. 12), owing to its square planer geometry, which enables it to strongly interact with cancer cellular DNA. Moreover, the endogenous copper ion can induces several mechanisms into the cancer cells including DNA interaction (intercalation, groove binding), oxidative cleavage, hydrolytic cleavage, Topoisomerase inhibition (TOPO I, II), and Proteasome inhibition (Santini et al., 2014).

On the other hand, Zn(II) complex displayed the greatest anti-liver cancer activity (IC50 3.92±0.85 μg/mL) that almost 2-times greater than the clinical drug (VBL) (IC50 6.83±0.75 μg/mL). This could be ascribed to the ability of the Zn(II) to block the hemeoxygenase inhibitor (HMOX1) which is produced in large amounts in solid tumors to help the cancer cell in defense against oxidative and other cellular stresses (Huang, Wallqvist and Covell, 2005). Interestingly, the Zn(II) complex is less cytotoxic than the other complexes and the clinical drug (VBL) (IC50 32.12±1.27 μg/mL) toward the normal liver cells (HL7702) (Fig. 11 C,D). Therefore, the new chemotherapeutic agent (Zn(II)H_2L) may of a promising anticancer candidate that can selectively trigger apoptosis in liver and colon carcinoma cells without harming the normal human cells.

4 Conclusion

A new series of Ni(II), Cu(II) and Zn(II) complexes of novel carbothioamide Schiff base ligand (H_2L, HL) have been prepared by reaction of ligand with metal(II) chlorides in 1:1 molar ratio. The coordination profiles of HL with M(II) ions, stoichiometry, and stereochemistry of metal complexes were investigated based upon various physicochemical and spectroscopic techniques. The thermal stability and surface morphological features of the free ligand and its coordination compounds have been studied using TGA, DTA, and SEM analysis. The comparative in-vitro anticancer studies revealed that all complexes are more cytotoxic than the parent ligands against human cancer cell lines (liver carcinoma ($HepG_2$), colon carcinoma (HCT116)), whereas, they exhibited lower toxicity as compared to the free ligand against normal liver cells (HL7702); signifying the importance of these complexes as new potential candidates to develop and explore novel chemotherapeutic agents in the field of cancer therapy. Particularly Zn(II)H_2L seems to be a superlative candidate as it the most cytotoxic one against $HepG_2$ concomitantly in lowest toxicity toward the normal human liver cells (HL7702), thus may offering a probable alternative to conventional chemotherapeutic agents.

References

[1] Y. Sunatsuki, Y. Motoda, and N. Matsumoto, "Copper(II) complexes with multidentate Schiff-base ligands containing imidazole groups: Ligand-complex or self-complementary molecule?," Coord. Chem. Rev., vol. 226, no. 1–2, pp. 199–209, 2002, doi: 10.1016/S0010-8545(01)00417-9.

[2] M. Galanski, "Recent Developments in the Field of Anticancer Platinum Complexes," Recent Pat. Anticancer. Drug Discov., vol. 1,

no. 2, pp. 285–295, 2008, doi: 10.2174/157489206777442287.

[3] S. V. Mamatha, M. Bhat, H. K. Kumara, D. Channe Gowda, M. Tirukoti, and S. K. Meenakshi, "Design, synthesis and SAR evaluation of mercaptooxadiazole analogs as anti-tubercular, anti-diabetic and anti-bacterial agents," Chem. Data Collect., vol. 26, p. 100343, 2020, doi: 10.1016/j.cdc.2020.100343.

[4] A. I. Khodair, "Glycosylation of 2-thiohydantoin derivatives. Synthesis of some novel S-alkylated and S-glucosylated hydantoins," Carbohydr. Res., vol. 331, no. 4, pp. 445–453, 2001, doi: 10.1016/S0008-6215(01)00040-4.

[5] L. K. Abdulrahman, M. M. Al-Mously, M. L. Al-Mosuli, and K. K. Al-Azzawii, "The biological activity of 5, 5′-Imidazolidine-2,4-Dione derivatives," Int. J. Pharm. Pharm. Sci., vol. 5, no. SUPPL.4, pp. 494–504, 2013.

[6] S. Ahmad, "Platinum-DNA interactions and subsequent cellular processes controlling sensitivity to anticancer platinum complexes," Chem. Biodivers., vol. 7, no. 3, pp. 543–566, 2010, doi: 10.1002/cbdv.200800340.

[7] A. S. Abdel-Aty, "Pesticidal Effects of Some Imidazolidine and Oxazolone Derivatives," World J. Agric. Sci., vol. 5, no. 1, pp. 105–113, 2009.

[8] M. Shiozaki, "Syntheses of hydantocidin and C-2-thioxohydantocidin," Carbohydr. Res., vol. 337, no. 21–23, pp. 2077–2088, 2002, doi: 10.1016/S0008-6215(02)00217-3.

[9] R. Al-Salahi, I. Alswaidan, H. A. Ghabbour, E. Ezzeldin, M. Elaasser, and M. Marzouk, "Docking and antiherpetic activity of 2-aminobenzo[de]-isoquinoline-1,3-diones," Molecules, vol. 20, no. 3, pp. 5099–5111, 2015, doi: 10.3390/molecules20035099.

[10] J. Seki, N. Shimada, K. Takahashi, T. Takita, T. Takeuchi, and H. Hoshino, "Inhibition of infectivity of human immunodeficiency virus by a novel nucleoside, oxetanocin, and related compounds.," Antimicrob. Agents Chemother., vol. 33, no. 5, pp. 773–775, 1989, doi: 10.1128/AAC.33.5.773.

[11] G. M. Shah, R. G. Shah, H. Veillette, J. B. Kirkland, J. L. Pasieka, and R. R. P. Warner, "Biochemical assessment of niacin deficiency among carcinoid cancer patients," Am. J. Gastroenterol., vol. 100, no. 10, pp. 2307–2314, 2005, doi: 10.1111/j.1572-0241.2005.00268.x.

[12] A. T. Baviskar et al., "N-fused imidazoles as novel anticancer agents that inhibit catalytic activity of topoisomerase IIα and induce apoptosis in G1/S phase," J. Med. Chem., vol. 54, no. 14, pp. 5013–5030, 2011, doi: 10.1021/jm200235u.

[13] J. A. Townsend, J. E. Keener, Z. M. Miller, J. S. Prell, and M. T. Marty, "Imidazole Derivatives Improve Charge Reduction and Stabilization for Native Mass Spectrometry," Anal. Chem., vol. 91, no. 22, pp. 14765–14772, 2019, doi: 10.1021/acs.analchem.9b04263.

[14] M. S. Saini, A. Kumar, J. Dwivedi, and R. Singh, "a Review : Biological Significances of Heterocyclic Compounds .," Int. J. Pharma Sci. Res., vol. 4, no. 3, pp. 66–77, 2013.

[15] A. M. S. Hebishy, M. S. Abdelfattah, A. Elmorsy, and A. H. M. Elwahy, "ZnO nanoparticles catalyzed synthesis of bis- and poly(imidazoles) as potential anticancer agents," Synth. Commun., vol. 50, no. 7, pp. 980–996, 2020, doi: 10.1080/00397911.2020.1726396.

[16] N. Muhammad and Z. Guo, "Metal-based anticancer chemotherapeutic agents," Curr. Opin. Chem. Biol., vol. 19, no. 1, pp. 144–153, 2014, doi: 10.1016/j.cbpa.2014.02.003.

[17] R. J. Sundberg, "Interactions of histidine and other imidazole derivatives with transition metal ions in chemical and biological systems," Chem. Rev., vol. 74, no. 4, pp. 471–517, 1974, doi: 10.1021/cr60290a003.

[18] R. Baková, M. Chergui, C. Daniel, A. Vlček Jr., and S. Záliš, "Relativistic effects in spectroscopy and photophysics of heavy-metal complexes illustrated by spin–orbit calculations of [Re(imidazole)(CO)3(phen)]+," Coord. Chem. Rev., vol. 255, no. 7–8, pp. 975–989, 2011, doi: 10.1016/j.ccr.2010.12.027.

[19] G. Spengler et al., "Biological activity of hydantoin derivatives on P-Glycoprotein (ABCB1) of mouse lymphoma cells," Anticancer Res., vol. 30, no. 12, pp. 4867–4872, 2010.

[20] A. A. E. Mourad, N. A. Farouk, E. S. H. El-Sayed, and A. R. E. Mahdy, "EGFR/VEGFR-2 dual inhibitor and apoptotic inducer: Design, synthesis, anticancer activity and docking study of new 2-thioxoimidazolidin-4one derivatives," Life Sci., vol. 277, no. April, p. 119531, 2021, doi: 10.1016/j.lfs.2021.119531.

[21] S. S. Kandil, G. B. El-Hefnawy, and E. A. Baker, "Thermal and spectral studies of 5-(phenylazo)-2-thiohydantoin and 5-(2-hydroxyphenylazo)-2-thiohydantoin complexes of cobalt(II), nickel(II) and copper(II)," Thermochim. Acta, vol. 414, no. 2, pp. 105–113, 2004, doi: 10.1016/j.tca.2003.11.021.

[22] H. Beyzaei, R. Aryan, and Z. Keshtegar, "Synthesis of New Imidazolidine and Tetrahydropyrimidine Derivatives," Adv. Chem., vol. 2014, no. Scheme 1, pp. 1–4, 2014, doi: 10.1155/2014/834641.

[23] H. Matsumura, K. Kojima, S. Mio, T. Yamamoto, A. Kodaira, and H. Koizumi, "Synthesis and characterization of a methacrylate monomer with a thiohydantoin structure," J. Oral Sci., vol. 62, no. 3, pp. 256–258, 2020, doi: 10.2334/josnusd.19-0005.

[24] J. M. Baruah, S. Kalita, and J. Narayan, "Green chemistry synthesis of biocompatible ZnS quantum dots (QDs): their application as potential thin films and antibacterial agent," Int. Nano Lett., vol. 9, no. 2, pp. 149–159, 2019, doi: 10.1007/s40089-019-0270-x.

[25] A. Di Santo, G. A. Echeverría, O. E. Piro, H. Pérez, A. Ben Altabef, and D. M. Gil, "Supramolecular architectures in luminescent Zn(II) and Cd(II) complexes containing imidazole derivatives: Crystal structures, vibrational and thermal properties, Hirshfeld surface analysis and electrostatic potentials," J. Mol. Struct., vol. 1134, no. Ii, pp. 492–503, 2017, doi: 10.1016/j.molstruc.2017.01.028.

[26] B. Marciniec et al., "Thermal study of four irradiated imidazoline derivatives in solid state," J. Therm. Anal. Calorim., vol. 88, no. 2, pp. 337–342, 2007, doi: 10.1007/s10973-006-8060-x.

[27] M. K. Trivedi, A. B. Dahryn Trivedi, and G. N. Gunin Saikia, "Physical and Structural Characterization of Biofield Treated Imidazole Derivatives," Nat. Prod. Chem. Res., vol. 03, no. 05, pp. 0–8, 2015, doi: 10.4172/2329-6836.1000187.

[28] C. Justin Dhanaraj and J. Johnson, "Synthesis, characterization, electrochemical and biological studies on some metal(II) Schiff base complexes containing quinoxaline moiety," Spectrochim. Acta - Part A Mol. Biomol. Spectrosc., vol. 118, pp. 624–631, 2014, doi: 10.1016/j.saa.2013.09.007.